Published in final edited form as:
Neuron. 2010 November 18; 68(4): 639–653. doi:10.1016/j.neuron.2010.09.024.

Single-Synapse Analysis of a Diverse Synapse Population: Proteomic Imaging Methods and Markers

Kristina D. Micheva, **Brad Busse**, **Nicholas C. Weiler**, **Nancy O'Rourke**, and **Stephen J Smith**
Department of Molecular and Cellular Physiology, Stanford University, Stanford, California 94305

Summary

A lack of methods for measuring the protein compositions of individual synapses *in situ* has so far hindered the exploration and exploitation of synapse molecular diversity. Here we describe the use of array tomography, a new high-resolution proteomic imaging method, to determine the composition of glutamate and GABA synapses in somatosensory cortex of Line-H-YFP Thy-1 transgenic mice. We find that virtually all synapses are recognized by antibodies to the presynaptic phosphoprotein synapsin I, while antibodies to 16 other synaptic proteins discriminate amongst 4 subtypes of glutamatergic synapses and GABAergic synapses. Cell-specific YFP expression in the YFP-H mouse line allows synapses to be assigned to specific presynaptic and postsynaptic partners and reveals that a subpopulation of spines on layer 5 pyramidal cells receives both VGluT1-subtype glutamatergic and GABAergic synaptic inputs. These results establish a means for the high-throughput acquisition of proteomic data from individual cortical synapses *in situ*.

Introduction

Rapidly accumulating physiological and genetic evidence establishes that the molecular diversity of synapses extends far beyond that envisioned by traditional classification schemes based solely on neurotransmitter identity. For instance, it is now clear that within each neurotransmitter category (e.g., glutamatergic, GABAergic, cholinergic) there is substantial diversity in the expression of many intrinsic synaptic proteins, including neurotransmitter transporters and receptors (Gupta et al., 2000; Hausser et al., 2000; Staple et al., 2000; Cherubini and Conti, 2001; Craig and Boudin, 2001; Cull-Candy et al., 2001; Grabowski and Black, 2001; Huang and Bergles, 2004; Mody and Pearce, 2004; Grant, 2006). Until synapse molecular diversity is properly fathomed, it is likely to be a troublesome source of variability in physiological and neurodevelopmental experimentation. Conversely, a systematic understanding of synapse diversity (i.e. the synaptome) is likely to provide valuable new perspectives on the organization of synaptic circuitry (i.e. the connectome), its development, plasticity and disorders. It is easy to envision, for instance, that a potential catalog of molecular synapse types (Grant, 2007) would help explorations of the synaptic basis of specific memory or disease processes to focus more fruitfully on specific synapse subpopulations.

Correspondence: kmicheva@stanford.edu (K.D.M.); sjsmith@stanford.edu (S.J S.).

To place a possible molecular catalog of synapse types on a firm footing, two broad experimental challenges remain. First, it is essential that synapse populations be explored at the single-synapse level. Until recently, the only way to reliably resolve and characterize individual synapses was by way of electron microscopy (EM). While traditionally a time-consuming and very volume-limited method, recent advances in EM (Denk and Horstmann, 2004; Harris et al., 2006; Knott et al., 2008; Anderson et al., 2009; Kasthuri and Lichtman, 2010) have greatly improved its throughput, even offering the possibility of detailed neuronal circuit reconstruction. Nonetheless, EM still provides only very limited proteomic discrimination (although Anderson et al., 2009, describe a very powerful new approach to integrating small-molecule discrimination with EM). Secondly, synapse diversity must be explored *in situ*, in ways that retain full fidelity to the intact tissue setting and allow for the acquisition of as much information as possible about circuit context and cellular morphology.

Array tomography (AT) is a high-resolution proteomic imaging method (Micheva and Smith, 2007; Micheva et al., 2010) that exploits a combination of light and EM approaches to resolve fine details at the level of synapses across large fields of view spanning entire circuits. Of prime significance to the present application, AT allows the immunofluorescence resolution of single synapses within cortical neuropil, where such resolution is highly problematic for other optical methods. Additionally, AT can acquire many more dimensions of immunofluorescence information about single synapses than previous methods (up to 17 in the present work, as compared to the standard immunofluorescence limit of three or four). AT also benefits from greatly improved quantitative reliability, since both staining and imaging are completely independent of depth within a tissue sample. Finally, AT delivers very high experimental throughput: our present automated methods acquire image data at a rate of approximately one million synaptic protein puncta per hour. Such throughput will help advance the analysis of synaptic diversity from the anecdote to the realm of solid bioinformatics. AT thus seems uniquely suited to meet the challenges of exploring the molecular diversity of cortical synapses.

Here, we describe array tomographic immunofluorescence methods for the single-synapse analysis of mouse cortex, focusing on the discrimination and analysis of glutamatergic and GABAergic synapses. Toward a goal of identifying every single cortical synapse as unambiguously as possible, we evaluated antibody markers to presynaptic proteins likely to be common to all synapses, such as synaptophysin, bassoon, and synapsin. We find that antibodies to the presynaptic phosphoprotein synapsin I (De Camilli et al., 1983; Hilfiker et al., 1999) are particularly robust and useful, labeling the vast majority of cortical synapses with a minimum of labeling at non-synaptic loci. For increased confidence in synapse identification, we also develop here a basis for conjoint use of multiple synaptic markers. We argue that antibodies to the glutamatergic synaptic proteins VGluT1, VGluT2, PSD-95, GluR2, NMDAR1 and the GABAergic synaptic proteins GAD, VGAT and gephyrin can be used both to distinguish reliably between glutamatergic and GABAergic synapses and begin the work of searching for finer synapse molecular subtypes within these broad categories.

Results

A note about color use

We have adopted a colorblind-friendly scheme in as many figures as possible. In figures with only two immunofluorescence channels (Figures 3, 6, 7, 8C,D) we use magenta and green as additive colors, such that regions of overlap display as white. When three or more channels need to be displayed (Figures 1, 2, 4 and 8A,B), we represent each channel with a non-transparent color plane. In this case, colors are non-additive, for example, white in such

figures is not the result of magenta and green overlap but rather a distinct color representing a distinct immunofluorescence channel.

AT resolves individual puncta of multiple synaptic proteins in mouse cortex

Figure 1 offers a panoramic view of a volume of somatosensory cortex from a YFP-H Thy-1 transgenic mouse (Feng et al., 2000) representative of the specimens used in the present work. The volume image rendered here was acquired by automated AT imaging of a mosaic of 52 fields per section over 60 serial sections (200 nm each) in three fluorescence spectral channels, comprising a total of 9,360 individual image tiles. The tiles were stitched and aligned in three-dimensions and rendered as described in *Methods*. This volume is 12 μm thick, 0.5 mm wide and extends a distance of 1.4 mm from the pial surface of the cortex through all cortical layers past the subcortical white matter and into a portion of the underlying striatum. The three fluorescence channels represented are YFP fluorescence (green), anti-tubulin (blue) and anti-synapsin I (magenta) immunofluorescence. The vast information content of the volume presented in Figure 1 is better appreciated from dynamic volume renderings as in Supplemental Movie S1.

YFP fluorescence in the cortex of line H mouse represents a soluble YFP marker transgenically expressed in a large subset of layer 5 pyramidal neurons. This mouse line was used because the YFP-expressing neurons provide a useful anatomical framework, with their apical dendrites extending all the way to layer 1 and their axons forming conspicuous bundles in the white matter. However, YFP fluorescence is not necessary for the subsequent single synapse analysis, which can be performed also in a wild type mouse. In addition to the YFP labeled neurons, the apical dendrites of pyramidal cells not expressing YFP are evident from tubulin immunostaining of their core microtubule bundles (Figure 1D). Finally, the presence of aggregates of synapsin I protein in the neuropil is apparent from the magenta puncta, which can be individually discerned (Figure 1C–H). The spatial distribution of synapsin immunoreactivity is consistent with that expected of neocortical synapses. For example, cell bodies appear as circular spaces largely devoid of synapsin puncta. The few puncta observed within such voids are actually situated in front or behind the cell bodies, as the depth of this volume is larger than the diameters of most cortical cell bodies. There is no staining in blood vessels and very few puncta in the white matter (Figure 1H). All of the data that follow were collected from arrays similar to that represented in Figure 1, but image acquisition was, for expediency's sake, carried out in single fields of view in layers 4 and 5, corresponding to the areas in Figure 1E and F, respectively. Thinner, 70 nm sections were used to increase z-resolution and the sampling of each synapse.

While the distribution of synapsin puncta resembles that of cortical synapses, it is not clear whether all synapsin puncta represent synapses and whether all synapses are immunoreactive for synapsin. Synapsin I is highly concentrated in presynaptic boutons (De Camilli et al., 1983) and has been used extensively as a general synaptic marker, but a one-to-one relationship between synapsin puncta and synapses has not yet been demonstrated. Therefore, it cannot be assumed that synapsin immunofluorescence data alone are sufficient for synapse identification. Also, there are other proteins, for example synaptophysin and bassoon, which are highly concentrated at presynaptic boutons and could be useful as general markers for synapses. To evaluate candidate cortical synapse markers, we developed a panel of antibodies that label a variety of pre- and postsynaptic proteins (Table 1, see Supplemental Experimental Procedures for antibody characterization). Because of the proteomic capability of AT to immunostain sections multiple times with different sets of antibodies, we were able to measure numerous pre- and postsynaptic markers at every putative synaptic locus. An example of multiple antibody labeling is shown in Figure 2, which represents a volume rendering from layer 4 of the somatosensory cortex of a YFP-H mouse immunostained with 10 different antibodies against synaptic proteins (synapsin,

bassoon, VGluT1, VGluT2, PSD95, GluR2, NMDAR1, GAD, VGAT, gephyrin) and one against tubulin. The sequence of antibody application is presented in Table S1 (dataset KDM-SYN-090416). In addition, two other fluorescent labels (YFP and DAPI) were imaged, making a total of 13 fluorescent channels collected from each section.

Synaptic protein distributions imaged by AT correlate as expected from synapse structure

Some of the antibody markers in Table 1 are expected to be present at all synapses in cortical neuropil, while others are specific for particular synapse subtypes. For example, as universal presynaptic proteins, synapsin and synaptophysin puncta overlap (Figure 3A). The majority of synapsin puncta also overlap with VGluT1, known to be present in most cortical glutamatergic synapses. In addition, synapsin puncta are closely apposed with PSD95 puncta as would be anticipated from imaging pre- and postsynaptic proteins at single synapses. GAD puncta, expected to label inhibitory GABAergic synapses, overlap with a small subset of synapsin puncta, and synapsin levels are generally lower in these synapses.

To quantify globally the extent of spatial correlation amongst various synaptic marker candidates, we designed a correlation matrix test based on the van Steensel method (van Steensel et al., 1996; see *Experimental Procedures* for full description). The basic idea is to test for the effect of very small relative displacements between pairs of marker images on a measurement of image overlap. Because of the abundance of many synaptic markers, overlapping spatial distributions might occur by chance. If the association between two channels is real, however, then any shift of one channel relative to the other will decrease the observed degree of colocalization. On the other hand, if two channels tend to be mutually exclusive, then a shift will increase the degree of colocalization. Finally, if the association between two channels is occurring by chance, then a shift will not substantially affect the degree of colocalization. Using a $20 \times 20 \times 6.3\ \mu m^3$ volume of neuropil from dataset KDM-SYN-091207 (Table S1), we computed a cross-correlation score for pairs of channels over a range of lateral offset distances. From the 17 antibodies used in this dataset, we focused on the general presynaptic markers synapsin, synaptophysin and bassoon, as well as several specific markers for glutamatergic (VGluT1, VGluT2, PSD95 and GluR2) and GABAergic synapses (GAD and VGAT).

The cross-correlation score is represented in Figure 3B as a grid of false colored squares with centers corresponding to the score at 0 offset and each pixel shift equal to 0.1 μm offset. To visualize the data, different channel pairs are also shown as immunofluorescent images from a small area of a single section of the same dataset. As can be seen in the correlation matrix, both synapsin and synaptophysin, and to a lesser extent bassoon, colocalize with all other synaptic markers, including those of smaller subsets of synapses that contain VGluT2 or GAD. All synaptic markers are anticorrelated with tubulin, which labels microtubules within dendrites and cell bodies. VGluT1 and VGluT2, found in cortical glutamatergic synapses, do not colocalize with the GABAergic markers. PSD95 and GluR2, both present at the postsynaptic side of glutamatergic synapses, correlate strongly with each other and more weakly with the presynaptic glutamatergic markers. GAD and VGAT, presynaptic markers for GABAergic synapses, show strong correlation. An interesting distinction can be made between the presynaptic markers with respect to their colocalization with postsynaptic markers. Presynaptic markers that are associated with synaptic vesicles (e.g. synapsin, synaptophysin, VGluTs) show high colocalization among themselves, while their colocalization with postsynaptic markers such as PSD95 and GluR2 is weaker. On the other hand, the presynaptic marker bassoon, which labels the presynaptic active zone, shows similar colocalization with both pre- and post-synaptic markers. This is due to the fact that the synaptic vesicle cluster is situated far enough from the postsynaptic density to be resolved by AT. On the other hand, the presynaptic active zone is only one synaptic cleft (around 20 nm) away from the postsynaptic density which is below the resolution

capabilities of AT. For example, in single section images in Figure 3B, synapsin puncta are seen next to PSD95 and GluR2 puncta, while bassoon overlaps with these postsynaptic markers.

AT immunofluorescence of synapsin is highly reliable as synapse marker

A single marker protein detectable at all synapses and only at synapses would be very useful for many purposes, but thus far there has been no conclusive demonstration of any such marker. While numerous markers, e.g., intrinsic proteins of synaptic vesicles, might be localized at every chemical synapse, the usefulness of any such antibody marker would be diminished if it were found at non-synaptic loci as well. From the colocalization matrix of Figure 3B, it is evident that both synapsin and synaptophysin colocalize strongly with all other synaptic markers and thus might be useful as general markers for synapses. Further examination of the immunofluorescence images revealed, however, that synaptophysin immunoreactivity is also fairly often detectable at obviously extrasynaptic sites, e.g., in cell body and dendritic cytoplasm and nuclei (Figure 3A). Synaptophysin puncta moreover tend to be smaller and less continuous than synapsin puncta. For these reasons, the synapsin I antibody appeared to be the stronger candidate as a reliable synaptic marker and was subjected to further evaluation.

Synapsin is detectable at virtually all dendritic spines—Almost all dendritic spines in adult cortex receive synapses and therefore a general synaptic marker should be present at these sites. To determine the distribution of synapsin puncta at spines, we reconstructed the apical dendrites of YFP-positive layer 5 pyramidal cells extending through layer 4 in tissue that was immunostained for both pre- and post-synaptic proteins (Figure 4).. Immunofluorescence reveals PSD95 puncta within spine heads that are closely associated with both synapsin and bassoon puncta. Two dendritic segments from dataset KDM-SYN-091207 were used to quantify the number of spines contacted by synapsin puncta. Only synaptic marker immunofluorescence within 0.5 μm of the YFP dendrites was considered for this analysis. One of the dendritic segments was 45 μm in length, 2 μm in width and had 131 spines (2.9 spines/μm). From the 116 spines included in their entirety within the imaged volume, 114 had at least one synapsin punctum associated with them. The other dendritic segment was 93 μm long, 1.7 μm wide and had 117 spines (1.3 spines/μm), from which 110 were completely included in the volume. All of these spines were associated with a synapsin punctum. Thus, more than 99% of the dendritic spines on layer 5 pyramidal neurons were in the immediate vicinity of a synapsin punctum. Moreover, other pre- and postsynaptic proteins colocalized with the synapsin puncta at these dendritic spines (100% of synapsin puncta with pre- and 98% with postsynaptic markers).

EM analysis supports the identification of synapses with synapsin immunoractivity—The use of the synapsin antibody as a general synaptic marker was also assessed at the EM level. Postembedding immunoEM using synapsin and a secondary antibody conjugated to colloidal gold (15 nm) labeled presynaptic boutons, as identified by the presence of synaptic vesicles and adjacent postsynaptic densities (Figure 5C). The relatively low density of immunogold labeling is likely due to the addition of 0.1% glutaraldehyde and 0.1% OsO_4 during tissue preparation, which is necessary for ultrastructural preservation but significantly impairs immunogenicity. Indeed, synapsin immunofluorescence on sections from tissue treated this way is much weaker than on our conventional sections used for the rest of this study (Figure S2).

We then compared synapsin immunofluorescence with the corresponding ultrastructure to assess what proportion of synapses identified at the EM level are fluorescently labeled. Because the tissue preparation for EM significantly reduces synapsin immunolabeling this

analysis will result in an underestimate of the presence of synapsin at synapses. Serial sections from tissue prepared for EM observation and mounted on coverslips were first immunofluorescently labeled with the synapsin antibody and imaged with the fluorescent microscope. The sections were then poststained with uranyl acetate and lead citrate and viewed in the SEM using the backscattered electron detector. The fluorescent and SEM images were aligned using the DAPI signal and the nuclei as viewed in the SEM. The bright DAPI-stained puncta in the nuclei correspond to the electron dense heterochromatin masses (Figure 5A,B). A comparison of the ultrastructurally identified synapses with synapsin immunofluorescence revealed that 91% of synapses (279 out of 305) were synapsin positive on at least one section. The intensity of synapsin immunofluorescence did not correlate with the size of the synapse as seen in the SEM. For example, some big presynaptic boutons (asterisk on Figure 5B) were very weakly labeled. Thus, despite the reduced immunoreactivity with conjugate immunofluorescence – SEM imaging, 91% of synapses were synapsin-positive, which is consistent with synapsin being a reliable marker for immunofluorescent imaging of cortical synapses.

Multiple synaptic proteins can be visualized volumetrically as a ‘synaptogram’ mosaic

The large number of immunofluorescence stains used with AT presents a challenge for visualization. The traditional color-coding cannot be used for so many channels, and volume reconstruction along any single axis can obscure weak labels or show false colocalization of markers. Therefore, we devised a representation for multi-channel volumetric image data, called a ‘synaptogram’ (Figure 6), that is useful for single-synapse analysis. All possible synaptic loci are identified with synapsin immunostaining and represented by single channel serial sections in a matrix where each section occupies a column and each channel a row. Sections represent a $1\times1\mu m^2$ area centered on the centroid of the synapsin punctum. With synaptograms many antibody labels can be visualized simultaneously and spatial relationships among labeled structures can be examined with precision and relative ease. For example, the synaptograms in Figure 6 use 18 different fluorescent signals: the general synaptic markers synapsin, synaptophysin and bassoon (2 different antibodies), 8 glutamatergic markers, 4 GABAergic markers and 2 structural markers (Dataset KDM-SYN-091207, Table S1). The glutamatergic synapse on the left has a distinct synaptogram appearance compared to the GABAergic synapse on the right. Both synapses contain the general synaptic markers synapsin, synaptophysin and bassoon. The glutamatergic synapse contains presynaptic VGluT1 as well as a number of postsynaptic scaffold and receptor markers (PSD95, MAGUK, GluR2, NMDA receptor subunits). The GABAergic synapse is distinguished by the presence of presynaptic GAD and VGAT as well as the postsynaptic scaffold protein gephyrin and GABAA receptor subunit. Both of the synapses are adjacent to a YFP-positive process and it appears that the glutamatergic synapse is making a contact with this process (postsynaptic markers overlap with the YFP signal), while the GABAergic synapse is not (postsynaptic markers away from the YFP process).

The synaptogram makes it easy to check for the continuity of a given marker punctum from one serial section to the next, and the 3D colocalization of multiple markers that would be expected at a true synapse. The synaptogram can also be useful in identifying fluorescence signals that are clearly not synaptic structures, such as staining artifacts, and excluding them from the analysis. For example, the presence of a synaptic vesicle immunofluorescence signal in just one isolated section is unlikely to originate from an actual synapse, because synaptic vesicle clusters almost always have a minimum extent greater than the 70 nm thickness.

AT imaging discriminates multiple glutamatergic and GABAergic synapse subtypes

To begin characterizing the diversity of cortical synapses we focused on a panel of 10 antibodies. Synapsin and bassoon were used as general synaptic markers. VGluT1, VGluT2, PSD95, GluR2 and NMDAR1 were used as markers for glutamatergic synapses. The vesicular glutamate transporters VGluT1 and VGluT2 were included because their expression reportedly varies depending on the intracortical or subcortical origins of the synapses. In particular it is believed that VGluT2 is predominantly expressed in thalamocortical synapses (Fremeau et al., 2001; De Gois et al., 2005; Graziano et al., 2008). GAD, VGAT and gephyrin were used as markers for GABAergic synapses. This combination of antibodies allowed the identification of two general types of synapses: glutamatergic and GABAergic, with the glutamatergic synapses further subdivided into subtypes containing VGluT1, both VGluT1 and 2, VGluT2 and other (lacking VGluT1 and 2) (Figure 7A).

Synapses formed by axons of layer 5 pyramidal neurons belonged to the glutamatergic VGluT1 subtype (Figure 7D), as evidenced by examination of YFP-positive presynaptic boutons. From 96 YFP synapses in layer 4 and 110 YFP synapses in layer 5, all had associated VGluT1, not VGluT2, immunofluorescence.

To further evaluate the reliability of our approach to single-synapse analysis, we calculated the proportion of synapses falling into each synaptic subtype from two experiments performed on tissue sections from the same region of the same animal, but with a different order of antibody application (Table S1, datasets KDM-SYN-090416 and KDM-SYN-091207). A cluster of glutamatergic markers was considered to be a synapse only if both pre- and postsynaptic markers were present. The requirement for the presence of pre- and postsynaptic markers was not applied to the GABAergic synapses, because it is not yet known whether the postsynaptic scaffold gephyrin is present at all synapses of this type (Fritschy et al., 2008). Instead, we adopted the less stringent criterion of colocalization of several presynaptic markers belonging to different compartments (e.g. cytoplasmic, presynaptic active zone and vesicular). Thus, in addition to the presence of a ubiquitous synaptic marker (e.g. synapsin or bassoon) and the cytoplasmic GAD, we required the presence of the vesicular marker VGAT, which has been shown to specifically localize to presynaptic boutons (Chaudhry et al., 1998). The results obtained from these 2 experiments were very similar (Table 2). Approximately 84% synapses were glutamatergic and 16% GABAergic. There were almost twice as many VGluT2 containing synapses (VGluT1 + 2 subtype and VGluT2 only subtype) in layer 4 compared to layer 5 (21.4% vs 12.9%). On average, only 4% of synapsin puncta were not associated with other synaptic proteins and therefore most likely do not represent synapses. The proportion of glutamatergic and GABAergic synapses, as well as the preference of VGlut2 synapses for layer 4 are consistent with previous studies (e.g. Micheva and Beaulieu, 1995;Fremeau et al., 2001;Graziano et al., 2008). These results, reproducible between 2 separate experiments, confirm the reliability of single-synapse analysis with AT. It should be noted that only one animal was analyzed quantitatively, and the results are aimed at evaluating the technique, not providing reference proportions of synapse types in the mouse somatosensory cortex. This will, undoubtedly, require a larger number of animals and is beyond the scope of the present study.

AMPA and NMDA receptors distributions vary at different glutamatergic synapses—There is great variability in the expression levels, subunit composition and localization of AMPA and NMDA receptors at synapses, which significantly affects their functional properties (e.g. Craig and Boudin, 2001). To further characterize cortical synapses based on the type of postsynaptic receptors present (Figure 7C), 110 synapses were

randomly selected in each of layers 4 and 5 using synapsin immunostaining. Inhibitory synapses were excluded from the analysis. The distribution of glutamatergic receptors was very similar in both cortical layers. The great majority of excitatory synapses contained both AMPA and NMDA receptors, as identified with antibodies against GluR2 and NMDAR1 respectively (85.4% in layer 4 and 84.5% in layer 5). In 11.8% of synapses in both layers only AMPA receptors could be detected and in 2.7% of synapses in layer 4 and 3.6% in layer 5 – only NMDA receptors. GluR2 and, to a lesser extent, NMDA labels often extended through more sections than PSD95, or were observed in sections adjacent to PSD labeling.

Synapsin is present at all glutamatergic and GABAergic synapses, but in varying amounts

In addition to enabling the study of synaptic diversity, the establishment of markers for synapse subtypes also allowed us to revisit the question of whether synapsin is expressed in all cortical synapses. From the conjugate immunofluorescence – SEM analysis it was observed that 91% of ultrastructurally identified synapses were labeled for synapsin, but, as mentioned before, those were suboptimal conditions for immunostaining. To better understand what proportion of synapses are labeled with synapsin in our tissue prepared for immunofluorescence, synapses were identified using different combinations of pre- and postsynaptic markers, excluding synapsin. Glutamatergic VGluT1 synapses were identified by the combination of VGluT1 - PSD-95 antibodies, VGluT2 synapses with VGluT2 - PSD-95 antibodies and GABAergic synapses with VGAT and gephyrin antibodies. One hundred synapses from each group were chosen randomly and the synapsin immunofluorescence associated with them was measured on all sections through the synapse. Synapsin immunofluorescence was above background levels in all analyzed synapses (Figure 7B). VGluT1 synapses contained the highest average synapsin levels (151 ± 7 arbitrary units) compared to VGluT2 (111± 7 a.u.) and VGAT synapses (81 ± 4 a.u.). A significant proportion of VGluT2 (17%) and VGAT synapses (12%) contained low levels of synapsin immunofluorescence (below 40 a.u.) compared to only 2% of the VGluT1 synapses.

These data further confirm that synapsin I can be used as a general synaptic marker because it appears to be present in all mouse glutamatergic and GABAergic cortical synapses. However, synapsin content as detected with immunofluorescence varies depending on synapse type with some VGluT2 and VGAT synapses exhibiting low levels of synapsin. Thus, applying a simple intensity threshold of synapsin immunofluorescence should be avoided because this can lead to underestimation of the synapse subtypes exhibiting low synapsin levels.

Double innervated spines on layer 5 pyramidal neurons are contacted by a VGluT1 and a GABAergic synapse

Double innervated dendritic spines are an intriguing synaptic arrangement involved in cortical plasticity and are found in a variety of species and cortical areas. Until now they have been observed only by EM (Jones and Powell, 1969; Micheva and Beaulieu, 1995; Knott et al., 2002; Jasinska et al., 2010). Very little is known about the identity of either the input or the target in this arrangement (Dehay et al., 1991; Kubota et al., 2007) especially in the mouse somatosensory cortex. AT can resolve neighboring synapses, as can be seen on Figure 5B, where adjacent synapses imaged in SEM are represented by separate immunofluorescent synapsin puncta. We therefore used AT to further characterize dually innervated spines. Examples of dendritic spines receiving 2 synaptic inputs, one glutamatergic and one GABAergic, are presented in Figure 8. These spines emerge from the apical dendrites of YFP-positive layer 5 pyramidal neurons. From 2 datasets (KDM-SYN-090416 and KDM-SYN-091207), 22 unequivocal double innervated spines were identified, i.e. both pre- and postsynaptic markers were present for the two inputs. Of those

spines, 82 % received a glutamatergic VGluT1 input and a GABAergic input. The remaining 18% received a glutamatergic VGluT2-containing (VGluT2 only, 9%, and VGluT1 and 2, 9%) as well as a GABAergic input. The great majority of the glutamatergic synapses contained both AMPA and NMDA receptors (91%), one spine was seen with NMDA receptors only, and one spine had neither AMPA nor NMDA receptor markers present. Thus, layer 5 pyramidal neurons have apical dendrites that contain spines innervated by both excitatory and inhibitory synapses, and the glutamatergic input to these spines is predominantly VGluT1-positive.

Discussion

Our results demonstrate that AT can be used for the efficient detection of individual synapses within brain tissue. Because of its proteomic capabilities and high resolution, AT allows a detailed characterization of individual synapses by their pre- and postsynaptic molecular composition, targets and spatial relationship to adjacent synapses. In addition, this technique can acquire very large volume images with high throughput which, together with a future development of advanced computational methods for data analysis, can provide for the first time the means for large-scale exploration of synaptic diversity.

In the present study, we identify a synapsin I antibody as a reliable marker for cortical synapses. Synapsin I associates exclusively with small synaptic vesicles and is concentrated in presynaptic boutons (De Camilli et al., 1983). The great majority of synapses are thought to contain synapsin and this protein has been used extensively as a general synaptic marker. However, the list of possible exceptions to this rule has grown recently and now includes ribbon synapses in the retina (Mandell et al., 1990), reticulogeniculate synapses (Kielland et al., 2006) and some GABAergic and VGluT2 containing synapses in the cerebral cortex (Bragina et al., 2007). AT, because of its increased sensitivity of immunofluorescence detection, ability to analyze multiple antibody stains and use immunofluorescence in conjunction with EM, allowed us to examine in detail the relationship between synapsin puncta and synapses in the mouse cerebral cortex.

For the synapsin antibody to be relied upon as a universal synapse marker, the following conditions had to be confirmed: 1) Synapsin labels the great majority of synapses; 2) Synapsin background labeling is minimal and can be differentiated from the labeling of synapses; and 3) Synapsin imaging has the resolution for discerning adjacent synapses. This study presents multiple lines of evidence that a rabbit polyclonal synapsin I antibody labels the vast majority of synapses in the mouse somatosensory cortex. For example, conjugate SEM of sections stained and imaged for synapsin immunofluorescence revealed that 91% of ultrastructurally identified synapses are immunofluorescently labeled on at least one section. Because the preparation of the tissue for EM sharply decreases antigenicity, this is a conservative estimate of the number of synapsin positive synapses. In tissue prepared for immunofluorescence, more than 99% of dendritic spines have an adjacent synapsin punctum. Also, all glutamatergic and GABAergic synapses identified by different combinations of pre- and postsynaptic markers contain synapsin label, albeit some at low levels. The background synapsin immunofluorescence is very low and only occasional puncta can be seen in cell body or large dendrite cytoplasm, or nuclei. Very few synapsin puncta (around 4%) exist alone, away from other synaptic markers. Synapsin immunofluorescence colocalizes with other presynaptic markers such as bassoon, VGluT1, VGluT2, VGAT and GAD and is also found immediately adjacent to postsynaptic markers such as PSD95, GluR2, NMDAR1 and gephyrin. These relationships were confirmed both at the synapse population level using a normalized cross-correlation analysis and for individual synapses using synaptograms. Finally, synapsin labeling with AT allows for the resolution of juxtaposed synapses as can be seen from conjugate EM. At the light level, when multiple

immunofluorescent labels are used, adjacent synaptic puncta can be observed that colocalize with different sets of pre- and postsynaptic antibodies and thus clearly belong to 2 different synapses.

The reliability of synapsin as a universal synaptic marker can be strengthened with the concomitant use of multiple strategically chosen synaptic markers. This not only helps the unequivocal identification of synapses, but also allows the positive identification of glutamatergic and GABAergic synapses within cortical neuropil and reveals the existence of several synaptic subtypes within those broad categories. Based on the presence of vesicular glutamate transporters, the glutamatergic synapses could be divided into those containing only VGluT1, only VGluT2, both VGluT1 and 2, and neither VGlut1 or 2. Synapsin immunofluorescence was detected in all synapses, but varied in intensity depending on the synapse type. It was highest in VGluT1 containing synapses, followed by VGluT2 synapses and GABAergic synapses. Previous studies (e.g. Bragina et al., 2007) have noted this heterogeneity of synapsin content in cortical synapses of rats. Using confocal microscopy in Vibratome sections, synapsin was observed in ~90% of VGluT1 puncta and only 30–50% of VGluT2 and VGAT puncta. This discrepancy with our results is probably due to the inability to detect small synapsin puncta using confocal microscopy. Previously, we observed fewer small synapsin puncta with confocal microscopy of Vibratome sections compared to AT on LR White sections prepared from the same animal (Micheva and Smith, 2007). The varying synapsin content in different synapse types is probably related to the different functional properties of the synapses. For example, release probability is low at VGluT1 synapses and high at VGluT2 (Fremeau et al., 2001) and many VGAT synapses (e.g. synapses made by parvalbumin-containing fast-spiking interneurons). Interestingly, there is evidence that synaptophysin is also expressed at a lower level in GABAergic synapses (Grønborg et al., 2010).

The proportions of different synaptic types was found to be very similar in layers 4 and 5, with the exception of VGluT2 containing synapses which, as observed in previous studies (Fremeau et al., 2001), were more prominently represented in layer 4. In addition, the existence of a sizable population of glutamatergic synapses that contain both VGluT1 and 2 was detected. There were several-fold more synapses containing both VGluT1 and 2 (15% in layer 4 and 10% in layer 5) than purely VGluT2 synapses (6% in layer 4 and 2.5% in layer 5). It was previously thought that the expression of VGluT1 and 2 in synapses in the adult animal is mostly complementary (Fremeau et al., 2001), but later studies have revealed the existence of both VGluTs in the same cortical synapses (Nakamura et al., 2007), particularly, the thalamocortical terminals in layer 4 (Graziano et al., 2008). VGluT1, VGluT1 and 2, and VGluT2 containing synapses appear to have distinct intracortical and subcortical origins, but the exact details of their identities are still being explored (Fremeau et al., 2001; De Gois et al., 2005; Graziano et al., 2008). Interestingly, the expression of the two vesicular glutamate transporters can be regulated by activity in opposite directions (De Gois et al., 2005). Thus, determining the VGluT1 and 2 content of synapses may provide information about their synaptic activity as well. Including more molecular markers in the single-synapse analysis is expected to reveal additional synaptic categories and contribute further to our understanding of synaptic diversity.

AT also allowed us to observe double innervated spines at the light level and to begin characterizing their input. The YFP fluorescence expressed in pyramidal neurons in the YFP-H mouse line conveniently outlines dendritic spines, but similar analysis can also be performed in wild type mice on neurons labeled by intracellular microinjections of fluorescent tracers or by *in utero* electroporation. Between 5 and 30% of cortical dendritic spines in a variety of species are thought to receive two synaptic inputs, one excitatory and one inhibitory (Jones and Powell, 1969; Le Vay and Gilbert, 1976; Micheva and Beaulieu,

1995). This intriguing synaptic arrangement is involved in cortical plasticity and is an example of a specific synapse subtype, namely inhibitory synapses on spines in layer 4, that changes in response to modifications in sensory experience and/or learning (Micheva and Beaulieu, 1995; Knott et al., 2002; Jasinska et al., 2010). Sensory deprivation induced by whisker removal results in a selective reduction of inhibitory synapses on spines, while increased sensory stimulation or classical conditioning involving the whiskers results in a selective increase in inhibitory synapses on spines. No direct evidence existed about the identity of either the dendritic spines or their inputs in mouse somatosensory cortex. A recent study in the frontal cortex of young rats suggests that double-innervated spines are preferentially targeted by VGluT2-containing thalamocortical afferents, while the inhibitory input is from all subtypes of cortical interneurons (Kubota et al., 2007). Using AT, we were able to observe the double innervated spines of layer 5 pyramidal neurons in mouse somatosensory cortex at the light level and confirm that they receive one glutamatergic and one GABAergic synapse. We also show for the first time that the glutamatergic input is predominantly VGluT1-containing and that both AMPA and NMDA receptors are present at the postsynaptic site. The addition of synaptic markers such as neuropeptide markers could provide information about the identity of the inhibitory input.

Conclusion

Here we demonstrate the usefulness of AT for the proteomic examination of individual synapses in natural brain tissue with full preservation of neuroanatomical and circuit context information. As efficient automated analysis strategies are developed to complement the inherently high throughput of array tomographic image acquisition, this tool should open new doors to the large-scale bioinformatic exploration of the molecular diversity and architecture of synapses. One likely consequence of such exploration could be the development of new schemes for the differentiation and cataloging of molecular synapse types. By isolating specific subsets of synapses, a synapse catalog could help enormously in pinpointing the specific synapse changes involved in particular neurological disorders (Luscher and Isaac, 2009) or forms of neural plasticity (Micheva and Beaulieu, 1995; Knott et al., 2002; Hofer et al., 2009; Xu et al., 2009; Yang et al., 2009). AT's unique abilities to extract simultaneously rich proteomic and fine-scale structural information also suggests that the method may substantially advance ongoing efforts to integrate the structural and molecular views of neuronal microcircuit function.

Experimental Procedures

Tissue preparation

All procedures related to the care and treatment of animals were approved by the Administrative Panel on Laboratory Animal Care at Stanford University. Four adult mice: three C57BL/6J and one YFP-H (Feng et al., 2000), were used for this study. The animals were anesthetized by halothane inhalation and their brains quickly removed and placed in 4% formaldehyde and 2.5% sucrose in phosphate-buffered saline (PBS) at room temperature. Each cerebral hemisphere was sliced coronally into 3 pieces and fixed and embedded using rapid microwave irradiation (PELCO 3451 laboratory microwave system with ColdSpot; Ted Pella, Redding CA) as described in Micheva et al, 2010. To preserve YFP fluorescence in the YFP-H mouse, the tissue was dehydrated only up to 70% ethanol.

For EM, the tissue was processed as above except that the fixative also contained 0.1 % glutaraldehyde and a postfixation step was added with osmium tetroxide (0.1%) and potassium ferricyanide (1.5%) with rapid microwave irradiation, 3 cycles of 1 min on −1 min off −1 min on at 100W, followed by 30 min at room temperature.

LRWhite sections

Ribbons of serial ultrathin (70 nm) sections were cut with an ultramicrotome (EM UC6, Leica Microsystems, Wetzlar, Germany) as described in (Micheva et al, 2010). The ribbons were mounted on subbed coverslips (coated with 0.5% gelatin and 0.05% chromium potassium sulphate) and placed on a hot plate (~ 60°C) for 30 min. For SEM imaging the subbed coverslips were also carbon coated using a Denton Bench Top Turbo Carbon Evaporator (Denton Vacuum, Moorestown, NJ). Subbed and carbon coated coverslips were also prepared for mounting ribbons of sections to be used for multiple immunostaining rounds (>6). For transmission electron microscope (TEM) the sections were collected on formvar coated nickel grids.

Immunofluorescence staining and antibodies

Staining was performed as described in (Micheva et al.,, 2010). The coverslips with sections were mounted using SlowFade Gold antifade with DAPI (Invitrogen, Carlsbad CA). To elute the applied antibodies, the mounting medium was washed away with dH_2O and a solution of 0.2M NaOH and 0.02% SDS in distilled water was applied for 20 min. After an extensive wash with Tris buffer and distilled water, the coverslips were dried and placed on a hot plate (60°C) for 30 min.

The primary antibodies and their dilutions are listed in Table 1. Only well characterized commercial antibodies were used and they were evaluated specifically for AT as described in Supplemental Experimental Procedures. For immunofluorescence, Alexa Fluor 488, 594 and 647 secondary antibodies of the appropriate species, highly pre-adsorbed (Invitrogen, Carlsbad CA) were used at a dilution 1:150. The sequence of antibody application in the multi-round staining is presented in Supplemental Table 1.

ImmunoEM staining

The staining protocol was similar to the immunofluorescence staining with the addition of 2 steps in the beginning: treatment for 1 min with saturated sodium metaperiodate solution in dH_2O to remove osmium and 5 min with 1% sodium borohydride in Tris buffer to reduce free aldehydes resulting from the presence of glutaraldehyde in the fixative. A 15 nm gold labeled goat anti-rabbit IgG secondary antibody (SPI Supplies, West Chester, PA) was used at 1:25 for 1h. After washing off the secondary antibody, the sections were treated with 1% glutaraldehyde for 1 min to fix the antibodies in place and the sections were poststained with 5% uranyl acetate for 30 min and lead citrate for 1 min.

Fluorescence microscopy and image processing

Sections were imaged on a Zeiss Axio Imager.Z1 Upright Fluorescence Microscope with motorized stage and Axiocam HR Digital Camera as described in Micheva et al., 2010. Briefly, a tiled image of the entire ribbon of sections on a coverslip was obtained using a 10x objective and the MosaiX feature of the software. The region of interest was then identified on each section with custom-made software and imaged at a higher magnification with a Zeiss 63x/1.4 NA Plan Apochromat objective, using the image-based automatic focus capability of the software. The resulting stack of images was exported to ImageJ, aligned using the MultiStackReg plugin and imported back into the Axiovision software to generate a volume rendering. When a ribbon was stained and imaged multiple times, the MultiStackReg plugin was used to align the stacks generated from each successive imaging session with the first session stacks based on the DAPI channel, then a second ‘within stack’ alignment was applied to all the stacks.

To reconstruct large volumes of tissue (Figure 1), we first used Zeiss Axiovision software to stitch together the individual high-magnification image tiles and produce a single ‘mosaic’

image of each antibody stain for each serial section in the ribbon. We created a z-stack of mosaic images for each fluorescence channel, and then grossly aligned the stacks using the MultiStackReg plugin. Finally, to remove non-linear physical warping introduced into the ribbons by the sectioning process, we used a second ImageJ plugin, autobUnwarpJ (available at http://www.stanford.edu/~nweiler), which adapts an algorithm for elastic image registration using vector-spline regularization (Arganda-Carreras et al., 2006).

For the figures, images representing single sections were upscaled using bicubic interpolation. No other image processing was used except for adjustment of brightness/contrast in some of the channels (NMDA receptor subunits and gephyrin). Synapsin immunofluorescence was not adjusted. For volume renderings, meant only for visual appreciation, more extensive image processing was used to adequately illustrate the spatial distribution and relationship between different markers. No quantifications or substantive comparisons were based on these images.

Colocalization analysis

To examine the spatial relationships between synaptic markers, we developed a colocalization detection function similar to the van Steensel method (van Steensel at al., 1996). Using a $20 \times 20 \times 6.3\ \mu m^3$ volume of neuropil, for each pair of channels we computed the three-dimensional normalized cross-correlogram (Lewis, 1995) for a range of lateral offsets approximating the size of a synapse, using Eaton's extension of the MATLAB function normxcorr2 (http://www.cs.ubc.ca/~deaton/tut/normxcorr3.html). Pairs of labeled channels with nonrandom associations (either positive or negative) should demonstrate a nonzero correlation effect which asymptotically approaches 0 at offset ranges exceeding their scale of interaction.

Transmission and Scanning electron microscopy

The immunostained TEM grids were imaged using a JEOL TEM1230 equipped with a Gatan 967 slow-scan, cooled CCD camera. For SEM following fluorescence imaging, the immunostained arrays were washed with dH_20 to remove the mounting medium and poststained with 5% uranyl acetate in H_20 for 30 min and lead citrate for 1 min. The arrays were imaged on a Zeiss Sigma scanning electron microscope equipped with field emission gun using the backscattered electron detector at 10kV. SEM images were aligned with the corresponding immunofluorescent images in ImageJ using the TurboReg plugin (Thevenaz et al., 1998). The nuclei as viewed with DAPI fluorescence and the SEM defined the identical regions in the two imaging modes.

Highlights

- Resolution of individual synapses *in situ* by high-throughput array tomography
- Measurement of multiple (e.g., 17) molecular markers at individual synapses
- Discrimination of defined subtypes of glutamate and GABA synapses
- Detection of both VGluT1-type glutamate and GABA synapses on single spines

Supplementary Material

Refer to Web version on PubMed Central for supplementary material.

Acknowledgments

This work was supported by grants from the National Institutes of Health (NS063210), Gatsby Charitable Trust, Howard Hughes Medical Institute, by funds from the Stanford's BioX Program, Stanford's Departments of Neurosurgery and Neurology and Neurological Science, and by a gift from Dr. Lubert Stryer. We thank Nafisa Ghori for her expert technical help and JoAnn Buchanan and Gordon Wang for help and advice. We thank Profs. Liqun Luo, Miriam Goodman and Thomas Clandinin (Stanford University) and Bradley Hyman (Harvard Medical School) for their very helpful comments on the manuscript.

References

Anderson JR, Jones BW, Yang JH, Shaw MV, Watt CB, Koshevoy P, Spaltenstein J, Jurrus E, UVK, Whitaker RT, Mastronarde D, Tasdizen T, Marc RE. A computational framework for ultrastructural mapping of neural circuitry. PLoS Biol 2009;7:e1000074. [PubMed: 19855814]

Bragina L, Candiracci C, Barbaresi P, Giovedi S, Benfenati F, Conti F. Heterogeneity of glutamatergic and GABAergic release machinery in cerebral cortex. Neuroscience 2007;146:1829–1840. [PubMed: 17445987]

Chaudhry FA, Reimer RJ, Bellocchio EE, Danbolt NC, Osen KK, Edwards RH, Storm-Mathisen J. The vesicular GABA transporter, VGAT, localizes to synaptic vesicles in sets of glycinergic as well as GABAergic neurons. J Neurosc 1998;18:9733–9750.

Cherubini E, Conti F. Generating diversity at GABAergic synapses. Trends Neurosci 2001;24:155–162. [PubMed: 11182455]

Craig AM, Boudin H. Molecular heterogeneity of central synapses: afferent and target regulation. Nat Neurosci 2001;4:569–578. [PubMed: 11369937]

Cull-Candy S, Brickley S, Farrant M. NMDA receptor subunits: diversity, development and disease. Curr Opin Neurobiol 2001;11:327–335. [PubMed: 11399431]

De Camilli P, Cameron R, Greengard P. Synapsin I (protein I), a nerve terminal-specific phosphoprotein. I. Its general distribution in synapses of the central and peripheral nervous system demonstrated by immunofluorescence in frozen and plastic sections. J Cell Biol 1983;96:1337–1354. [PubMed: 6404910]

De Gois S, Schäfner MKH, Defamie N, Chen C, Ricci A, Weihe E, Varoqui H, Erickson JD. Homeostatic scaling of vesicular glutamate and GABA transporter expression in rat neocortical circuits. J Neurosci 2005;25:7121–7133. [PubMed: 16079394]

Dehay C, Douglas RJ, Martin KAC, Nelson C. Excitation by geniculocortical synapses is not 'vetoed' at the level of dendritic spines in cat visual cortex. J Physiol 1991;440:723–734. [PubMed: 1804984]

Denk W, Horstmann H. Serial block-face scanning electron microscopy to reconstruct three-dimensional tissue nanostructure. PLoS Biol 2004;2:e329. [PubMed: 15514700]

Feng G, Mellor RH, Bernstein M, Keller-Peck C, Nguyen QT, Wallace M, Nerbonne JM, Lichtman JW, Sanes JR. Imaging neuronal subsets in transgenic mice expressing multiple spectral variants of GFP. Neuron 2000;28:41–51. [PubMed: 11086982]

Fremeau R, Troyer M, Pahner I, Nygaard G, Tran C, Reimer R, Bellocchio E, Fortin D, Storm-Mathisen J, Edwards R. The expression of vesicular glutamate transporters defines two classes of excitatory synapse. Neuron 2001;31:247–260. [PubMed: 11502256]

Fritschy JM, Harvey RJ, Schwarz G. Gephyrin: where do we stand, where do we go? Trends Neurosci 2008;31:257–264. [PubMed: 18403029]

Grabowski PJ, Black DL. Alternative RNA splicing in the nervous system. Prog Neurobiol 2001;65:289–308. [PubMed: 11473790]

Grant SG. The synapse proteome and phosphoproteome: a new paradigm for synapse biology. Biochem Soc Trans 2006;34:59–63. [PubMed: 16417483]

Grant SG. Toward a molecular catalogue of synapses. Brain Res Rev 2007;55:445–449. [PubMed: 17572504]

Graziano A, Liu XB, Murray KD, Jones EG. Vesicular glutamate transporters define two sets of glutamatergic afferents to the somatosensory thalamus and two thalamocortical projections in the mouse. J Comp Neurol 2008;507:1258–1276. [PubMed: 18181146]

Grønborg M, Pavlos NJ, Brunk I, Chua JJ, Münster-Wandowski A, Riedel D, Ahnert-Hilger G, Urlaub H, Jahn R. Quantitative comparison of glutamatergic and GABAergic synaptic vesicles unveils selectivity for few protins including MAL2, a novel synaptic vesicle protein. J Neurosci 2010;30:2–12. [PubMed: 20053882]

Gupta A, Wang Y, Markram H. Organizing principles for a diversity of GABAergic interneurons and synapses in the neocortex. Science 2000;287:273–278. [PubMed: 10634775]

Harris KM, Perry E, Bourne J, Feinberg M, Ostroff L, Hurlburt J. Uniform serial sectioning for transmission electron microscopy. J Neurosci 2006;26:12101–12103. [PubMed: 17122034]

Hausser M, Spruston N, Stuart GJ. Diversity and dynamics of dendritic signaling. Science 2000;290:739–744. [PubMed: 11052929]

Hilfiker S, Pieribone VA, Czernik AJ, Kao HT, Augustine GJ, Greengard P. Synapsins as regulators of neurotransmitter release. Philos Trans R Soc Lon B Biol Sci 1999;354:269–279. [PubMed: 10212475]

Hofer SB, Mrsic-Flogel TD, Bonhoeffer T, Hübener M. Experience leaves a lasting structural trace in cortical circuits. Nature 2009;457:313–317. [PubMed: 19005470]

Huang YH, Bergles DE. Glutamate transporters bring competition to the synapse. Curr Opin Neurobiol 2004;14:346–352. [PubMed: 15194115]

Jones EG, Powell TP. Morphological variations in the dendritic spines of the neocortex. J Cell Sci 1969;5:509–529. [PubMed: 5362339]

Jasinska M, Siucinska E, Cybulska-Klosowicz A, Pyza E, Furness DN, Kossut M, Glazewski S. Rapid, learning-induced inhibitory synaptogenesis in murine barrel field. J Neurosci 2010;30:1176–1184. [PubMed: 20089926]

Kasthuri N, Lichtman JW. Neurocartography. Neuropsychopharmacology 2010;35:342–343. [PubMed: 20010709]

Kielland A, Erisir A, Walaas SI, Heggelund P. Synapsin utilization differs among functional classes of synapses on thalamocortical cells. J Neurosci 2006;26:5786–5793. [PubMed: 16723536]

Knott G, Marchman H, Wall D, Lich B. Serial section scanning electron microscopy of adult brain tissue using focused ion beam milling. J Neurosci 2008;28:2959–2964. [PubMed: 18353998]

Knott GW, Quairiaux C, Genoud C, Welker E. Formation of dendritic spines with GABAergic synapses induced by whisker stimulation in adult mice. Neuron 2002;34:265–273. [PubMed: 11970868]

Kubota Y, Hatada S, Kondo S, Karube F, Kawaguchi Y. Neocortical inhibitory terminals innervate dendritic spines targeted by thalamocortical afferents. J Neurosci 2007;27:1139–1150. [PubMed: 17267569]

Le Vay S, Gilbert CD. Laminar patterns of geniculocortical projection in the cat. Brain Res 1976;113:1–19. [PubMed: 953720]

Lewis JP. Fast Normalized Cross-Correlation. Industrial Light and Magic. 1995

Luscher C, Isaac JT. The synapse: center stage for many brain diseases. J Physiol 2009;587:727–729. [PubMed: 19074963]

Mandell JW, Townes-Anderson E, Czernik AJ, Cameron R, Greengard P, De Camilli P. Synapsins in the vertebrate retina: absence from ribbon synapses and heterogeneous distribution among conventional synapses. Neuron 1990;5:19–33. [PubMed: 2114884]

Micheva KD, Beaulieu C. An anatomical substrate for experience-dependent plasticity of the rat barrel field cortex. Proc Natl Acad Sci U S A 1995;92:11834–11838. [PubMed: 8524859]

Micheva KD, Smith SJ. Array tomography: a new tool for imaging the molecular architecture and ultrastructure of neural circuits. Neuron 2007;55:25–36. [PubMed: 17610815]

Micheva, KD.; O'Rourke, N.; Busse, B.; Smith, SJ. Optical imaging techniques: A laboratory manual. Cold Spring Harbor Laboratory Press; 2010. Array tomography: High-resolution 3D immunofluorescence. (in press)

Mody I, Pearce RA. Diversity of inhibitory neurotransmission through GABA(A) receptors. Trends Neurosci 2004;27:569–575. [PubMed: 15331240]

Nakamura K, Watakabe A, Hioki H, Fujiyama F, Tanaka Y, Yamamori T, Kaneko T. Transiently increased colocalization of vesicular glutamate transporters 1 and 2 at single axon terminals during

postnatal development of mouse neocortex: a quantitative analysis with correlation coefficient. Eur J Neurosci 2007;26:3054–3067. [PubMed: 18028110]

Staple J, Morgenthaler F, Catsicas S. Presynaptic heterogeneity: Vive la difference. News Physiol Sci 2000;15:45–49. [PubMed: 11390875]

Thevenaz P, Ruttimann UE, Unser M. A pyramid approach to subpixel registration based on intensity. IEEE Trans Image Process 1998;7:27–41. [PubMed: 18267377]

van Steensel B, Binnendijk EP, Hornsby CD, van der Voort HT, Krozowski ZS, de Kloet ER, van Driel R. Partial colocalization of glucocorticoid and mineralocorticoid receptors in discrete compartments in nuclei of rat hippocampus neurons. J Cell Sci 109:787–792. [PubMed: 8718670]

Xu T, Yu X, Perlik AJ, Tobin WF, Zweig JA, Tennant K, Jones T, Zuo Y. Rapid formation and selective stabilization of synapses for enduring motor memories. Nature 2009;462:915–919. [PubMed: 19946267]

Yang G, Pan F, Gan WB. Stably maintained dendritic spines are associated with lifelong memories. Nature 2009;462:920–924. [PubMed: 19946265]

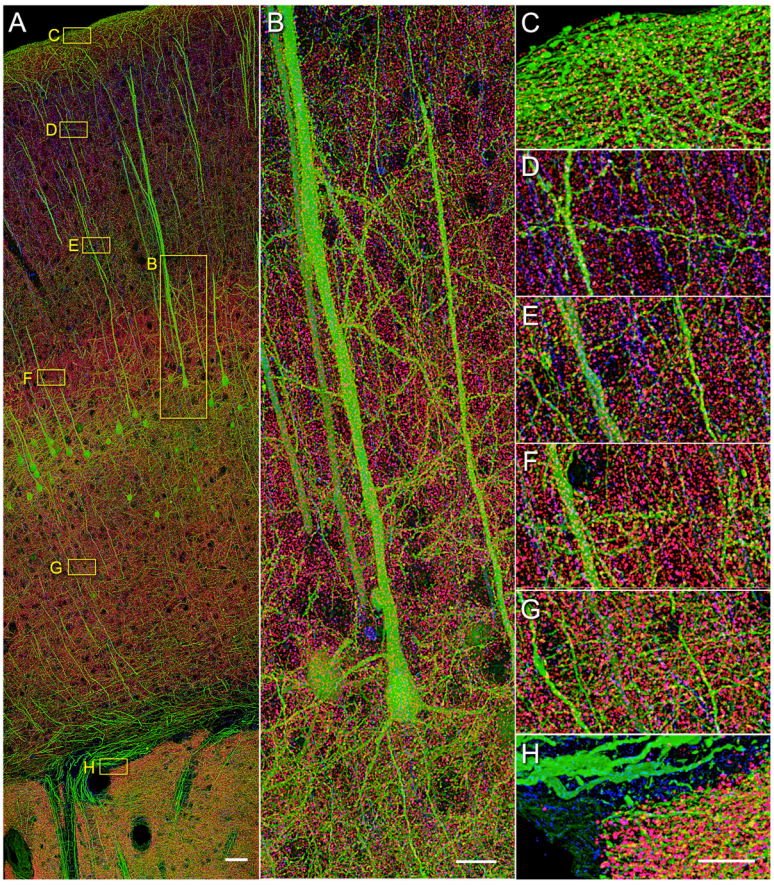

Figure 1.

Array tomographic synapsin I immunofluorescence in the cerebral cortex of an adult YFP-H mouse is punctate and consistent with synapse identity. (A) A volume rendering of 60 serial sections (200 nm each) through the entire cortical depth, including portions of the striatum. While all subsequent experiments and analysis were performed on thinner, 70 nm sections, the thicker sections in this case have allowed us to collect a larger volume and to better visualize the extensive dendrites of pyramidal neurons. Synapsin (magenta), tubulin (blue), and YFP (green). Scale bar, 50 μm. (B) A close up of layer 5 pyramidal neurons labeled with YFP. (C–H) Zoomed-in view of layers 1 (C), 2/3 (D), 4 (E), 5a (F), 6a (G) and white matter and striatum (H). Scale bar for B–H, 10 μm. See also Movie S1 for a more revealing rendering of the same image volume and Figure S1 for comparison of different synapsin antibodies.

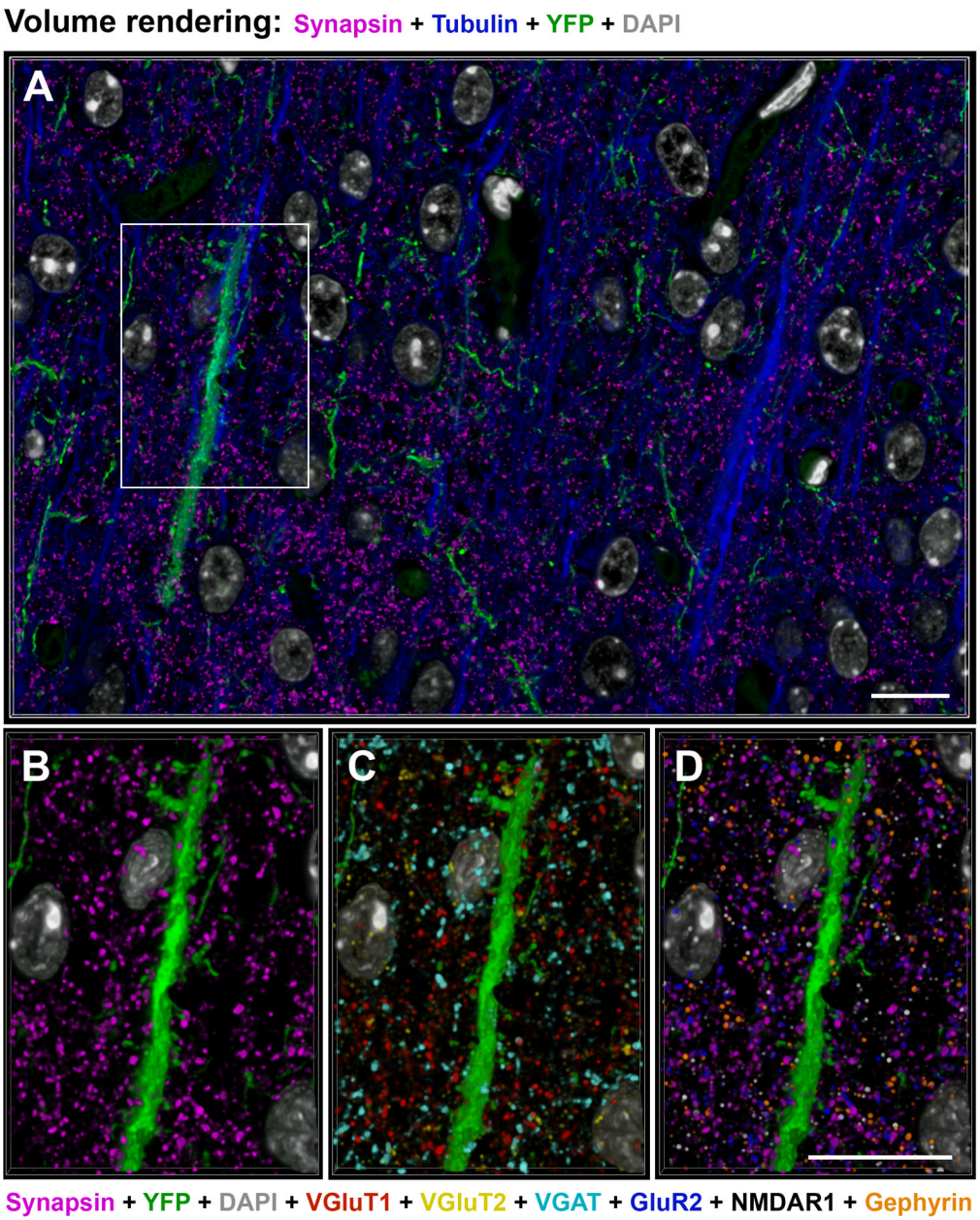

Figure 2.

Proteomic immunofluorescence AT of mouse somatosensory cortex yields staining patterns consistent with synaptic protein distributions. Volume rendering from 20 sections, 70 nm each, from an array stained with 11 antibodies (Table S1, dataset KDM-SYN-09041). (A) Tubulin (blue), synapsin (magenta), YFP (green) and DAPI (grey) fluorescence. (B–D) The boxed area in (A). DAPI (grey) and YFP (green). (B) Distribution of all presynaptic boutons as labeled with synapsin (magenta). (C) Distribution of VGluT1 (red), VGluT2 (yellow) and GAD (cyan) presynaptic boutons. (D) Postsynaptic labels: GluR2 (blue), NMDAR1 (white) and gephyrin (orange) next to synapsin (magenta). Scale bar 10 μm. See also Table S1 for sequence of antibody application.

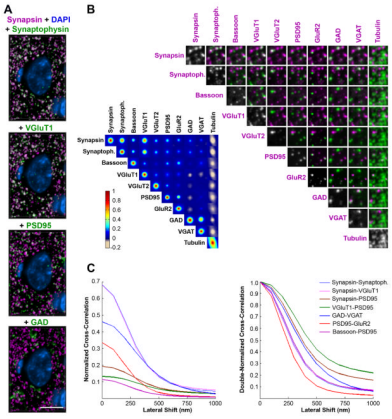

Figure 3.

Multiple synaptic proteins are colocalized in a fashion consistent with synaptic identity and glutamatergic and GABAergic synapse subtype. (A) Volume rendering of 20 sections (70 nm) from the mouse somatosensory cortex immunostained for synapsin (magenta) and synaptophysin, VGluT1, PSD95 or GAD (green). Colocalization of the magenta and green channels is displayed as white. DAPI, blue. These volume renderings are from an array stained with 17 antibodies (Table S1, dataset KDM-SYN-091207). Scale bar, 5 μm. (B) Colocalization matrix of nine synaptic markers and tubulin (left) and corresponding pair-wise representation of the channels on a small area (4 × 4 μm) of a single section (right). For each pair of channels we computed a cross-correlation score over a range of lateral offset distances for images in the two channels. The cross-correlation score is represented as a grid of false colored squares with their center representing the score at 0 offset and each pixel equal to 0.1 μm offset. (C) For a subset of channel comparisons, the cross-correlation score is plotted as a function of the lateral offset. Each trace is obtained by averaging 16 equally-spaced radii. Left, With no lateral shift the normalized cross-correlation is equal to the Pearson correlation coefficient, and at shifts beyond the rough size of a synapse the correlation drops to ~ 0 for all channels. Right, The same is normalized such that each curve is 1.0 in the no-shift case. Pre-presynaptic and post-postsynaptic channel comparisons drop off sharply, while pre-postsynaptic do not.

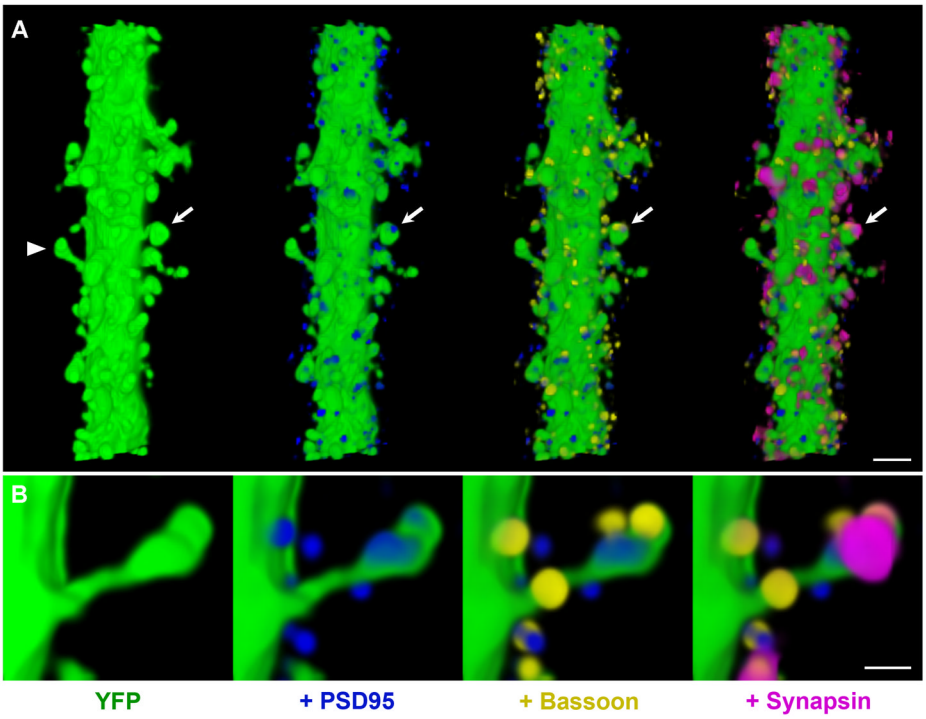

Figure 4.

Dendritic spines in mouse cerebral cortex are contacted by synapsin puncta and colocalize with other pre- and postsynaptic markers. Volume rendering of 45 sections from dataset NAOR-081118 (Table S1). To better visualize the synaptic markers associated with dendritic spines, only immunofluorescence within 0.5 μm of the YFP dendrite was displayed. (A) In the left panel, a 20 μm long segment from a spiny dendrite of a layer 5 pyramidal cell (green) is shown as it traverses layer 4. In each subsequent panel the labeling of a synaptic protein is added. PSD95 (blue), bassoon (yellow), and synapsin (magenta). The postsynaptic protein PSD95 is found within spine heads and closely apposed to the presynaptic proteins bassoon and synapsin (arrow). Scale bar, 2 μm. (B) The opposite side of the spine marked with an arrowhead in (A) at higher magnification. Scale bar, 0.5 μm.

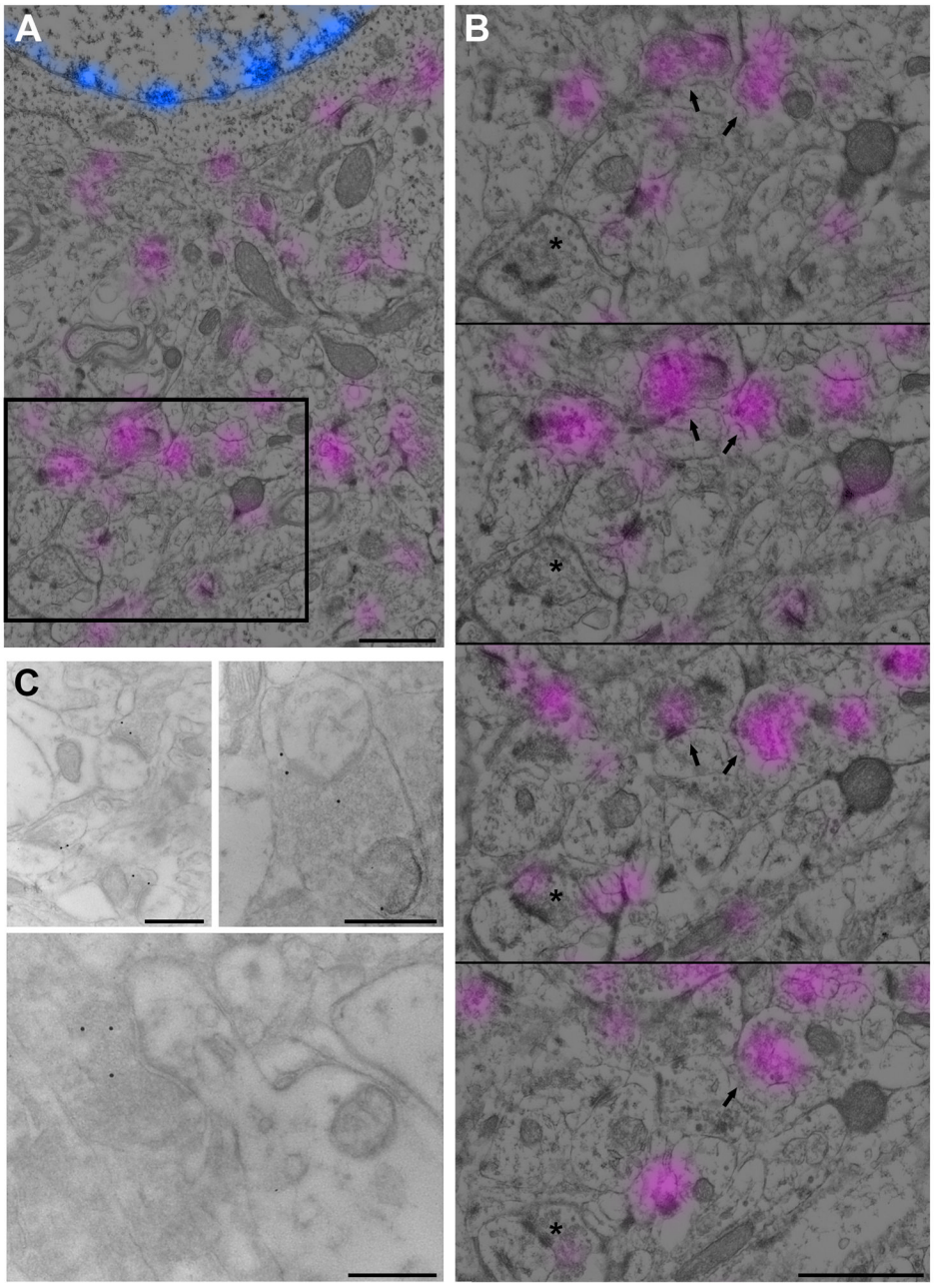

Figure 5.

Ultrastructurally identified synapses are labeled with the synapsin antibody. (A, B) Conjugate synapsin immunofluorescence and SEM of the adult mouse cerebral cortex. Synapsin (magenta) and DAPI (blue) signal as obtained with the fluorescence microscope are overlaid on the SEM image from the same section. (B) Four serial sections through the boxed region in (A). Boxed region is section #2 in the series. The majority of presynaptic boutons are consistently labeled from section to section (arrows), but some are labeled only on few sections with a weak signal (asterisk). Scale bar, 0.5 μm. (C) A TEM image of postembedding gold immuno-EM for synapsin. The 15 nm gold particles label presynaptic terminals as identified by the presence of synaptic vesicles and postsynaptic density. Scale bar, 0.5 μm. See also Figure S2 for effect of tissue processing on synapsin immunostaining.

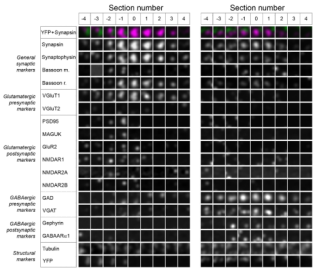

Figure 6.

Synaptograms are useful for viewing proteomic information from serially sectioned single synapses. A glutamatergic (left) and a GABAergic synapse (right) are shown. Each square represents an area of 1×1 μm from a single 70 nm section. Each section through the synapsin punctum occupies a column and each antibody label – a row. See also Table S1 for sequence of antibody application.

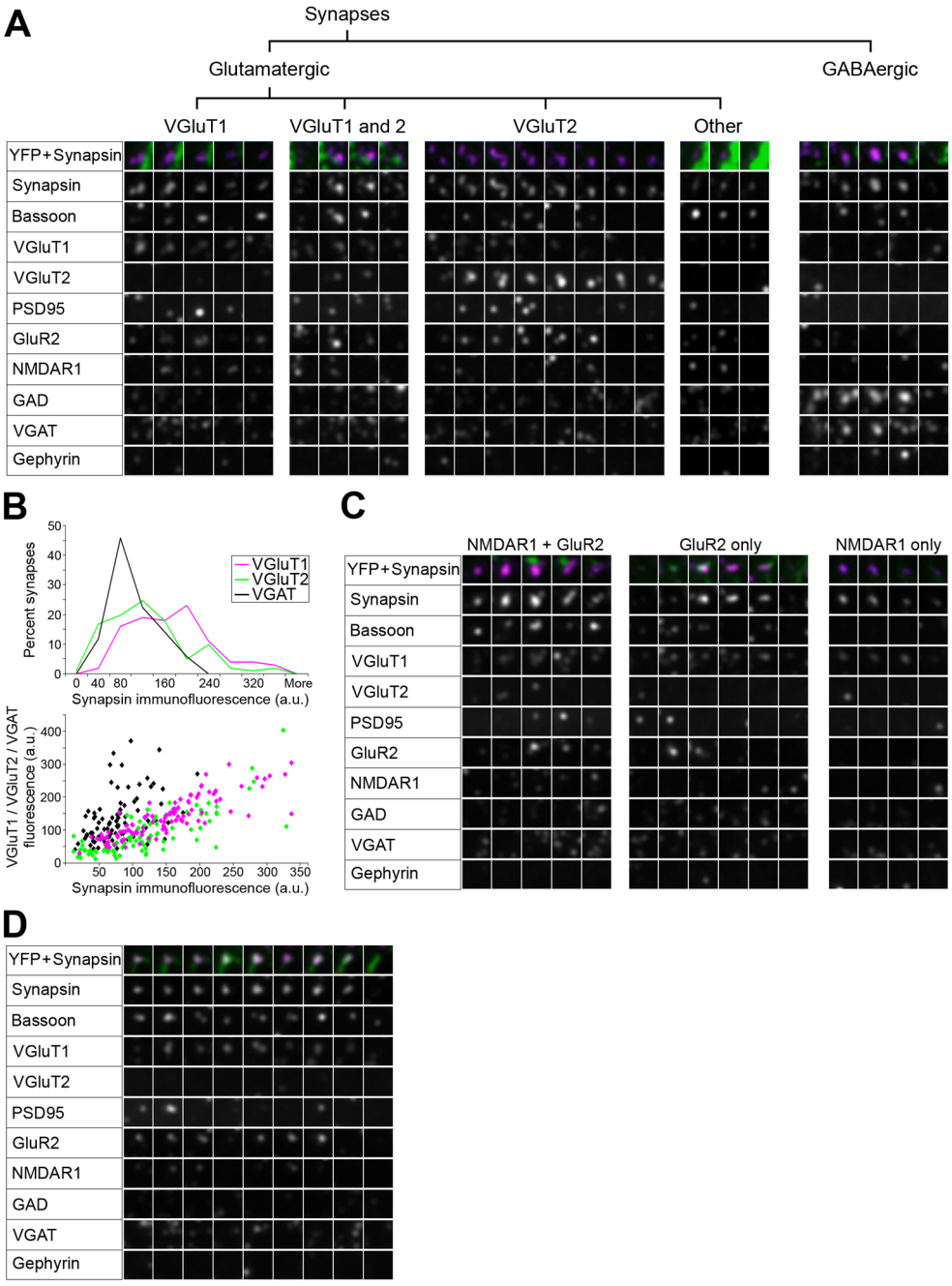

Figure 7.

Proteomic imaging with AT reveals the diversity of cortical synapses. (A) Examples of synaptograms representing the main synapse subtypes observed in mouse somatosensory cortex with the current antibody panel. (B) Synapsin content of different synaptic subtypes. For each subtype, 100 synapses were randomly selected using the VGluT1-PSD95, VGluT2-PSD95 and VGAT-gephyrin channels and synapsin immunofluorescence was measured on each section through the synapse. Top panel, Histograms of synapsin immunofluorescence in the three synapse subtypes. Lower panel, Scatterplot of synapsin intensity versus the respective vesicular transporter immunofluorescence for each synapse. (C) Examples of

glutamatergic synapses with different postsynaptic receptor combinations. (D) Example of a synapse made by the axon of a YFP-positive layer 5 pyramidal neuron.

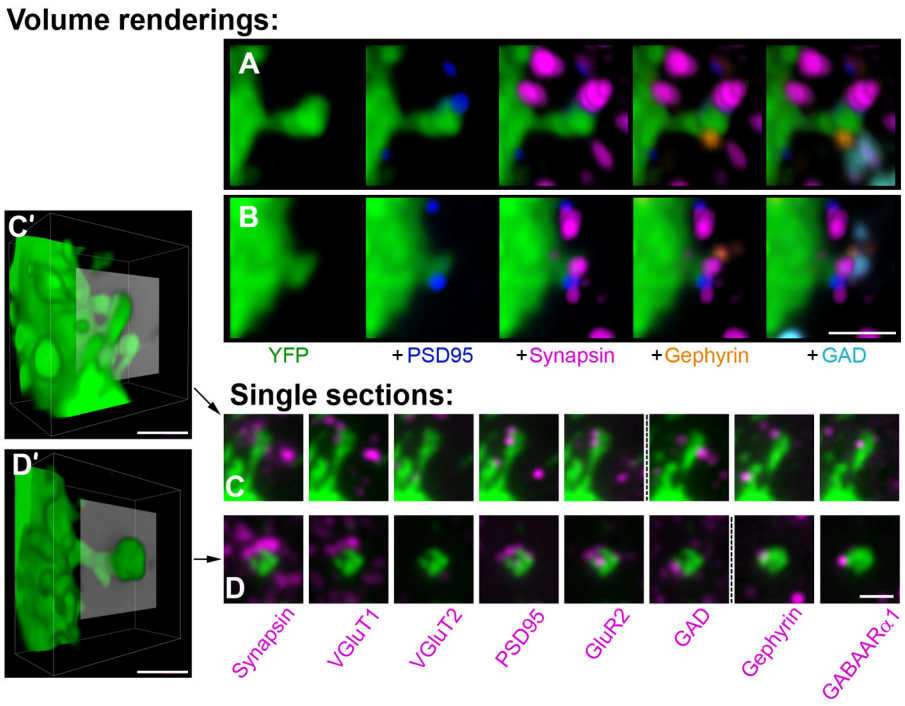

Figure 8.

Double innervated spines receive both a glutamatergic VGluT1 and GABAergic synapse. (A, B) Volume rendering of dendritic spines from YFP-positive pyramidal cell dendrites (green), each receiving 2 synaptic inputs on the head. The glutamatergic synapses are represented by postsynaptic PSD95 label (blue) and presynaptic synapsin (magenta). The GABAergic synapses are represented by postsynaptic gephyrin (orange) and presynaptic GAD (cyan). The labels are added consecutively from left to right. Additional synapses not contacting the spines are also observed within the reconstructed volume. (C, D), Single sections through double innervated spines labeled with multiple antibodies. For each spine the two adjacent sections where most of the markers were present was chosen. Each panel shows the spine (green) and one synaptic marker (magenta). Direct overlap of the two labels is seen as white. The punctuated line separates adjacent sections. C′ and D′ show a volume rendering of the spines in C and D with the plane of the single sections represented in gray. Scale bar, 1 μm.

Table 1

Synaptic antibodies used in this study. See also Figure S3.

	Antibody	Antigen localization	Species	Source	Cat. No.	Dilution
All synapses	Synapsin I	presynaptic	Rabbit	Millipore	AB1543P	1:100
	Bassoon	presynaptic	Mouse	Abcam	ab13249	1:100
	Bassoon	presynaptic	Rabbit	Synaptic Systems	141003	1:100
	Synaptophysin	presynaptic	Mouse	Abcam	ab8049	1:10
	Synaptophysin	presynaptic	Rabbit	Abcam	ab68851	1:100
Glutamatergic	VGluT1	presynaptic	Mouse	NeuroMab	75-066	1:100
	VGluT1	presynaptic	Guinea Pig	Millipore	AB5905	1:1000
	VGluT2	presynaptic	Guinea Pig	Millipore	AB2251	1:1000
	PSD-95	postsynaptic	Mouse	NeuroMab	75-028	1:100
	panMAGUK	postsynaptic	Mouse	NeuroMab	75-029	1:100
	GluR2	postsynaptic	Mouse	Millipore	MAB397	1:50
	GluR2/3	postsynaptic	Rabbit	Millipore	AB1506	1:100
	NMDAR1	postsynaptic	Mouse	Millipore	MAB363	1:200
	NMDAR2A	postsynaptic	Mouse	Millipore	MAB5216	1:25
	NMDAR2B	postsynaptic	Mouse	NeuroMab	75-101	1:500
	GAD	presynaptic	Rabbit	Millipore	AB1511	1:300
GABAergic	VGAT	presynaptic	Mouse	Synaptic Systems	131 011	1:100
	Gephyrin	postsynaptic	Mouse	BD Biosciences	612632	1:100
	GABAARα1	postsynaptic	Mouse	NeuroMab	75-136	1:100

Table 2

Proportion of synapses from different synaptic subtypes.

Synaptic subtype	Layer 4		Layer5	
	Exp. 1	Exp. 2	Exp. 1	Exp. 2
VGluT1	60.1% (149)	57.5% (100)	66.7% (156)	67.3% (113)
VGluT1+2	15.3% (38)	15.5% (27)	9.0% (21)	11.9% (20)
VGluT2	5.6% (14)	6.3% (11)	2.6% (6)	2.4% (4)
Other glutamatergic	3.6% (9)	4.6 (8)	5.6% (13)	2.4% (4)
GABAergic	15.3% (38)	16.1 (28)	16.2% (38)	16.1% 27)
All synapses	100% (248)	100% (174)	100% (234)	100% (168)
All synapsin puncta	262	183	242	172
Not synapse	5.3% (14)	4.9% (9)	3.3% (8)	2.3% (4)